Cement and Concrete Research 42 (2012) 1286–1297

Contents lists available at SciVerse ScienceDirect

Cement and Concrete Research

journal homepage: http://ees.elsevier.com/CEMCON/default.asp

Evaluation of the effects of drying shrinkage on the behavior of concrete structures strengthened by overlays

Y. Theiner *, G. Hofstetter

Institute of Basic Sciences in Civil Engineering, University of Innsbruck, Technikerstraße 13, A-6020 Innsbruck, Austria

ARTICLE INFO

Article history:
Received 18 October 2011
Accepted 6 June 2012

Keywords:
Concrete (E)
Drying (A)
Humidity (A)
Shrinkage (C)
Mass water content

ABSTRACT

The present contribution focuses on the experimental evaluation of the effects of drying shrinkage on the behavior of concrete structures strengthened by overlays. To this end a comprehensive laboratory test program is presented. Tests on thin concrete slices served for determining the water desorption isotherm and the ultimate drying shrinkage strains. The time and depth dependent mass water content distributions and the evolution of the drying shrinkage strains were measured on concrete prisms and on larger brick-shaped concrete specimens during two years of drying. After two years of drying the brick-shaped specimens were supplemented by a concrete overlay. Measurements of the mass water content distribution were continued during water jetting and subsequent wetting of the top surface. In addition, the shrinkage strains were recorded in the composite specimens during subsequent drying.

1. Introduction

Shrinkage is the time-dependent volume decrease of concrete without the action of external loads. It is caused by chemical, thermal and hygral processes. Basically, four different types of shrinkage can be distinguished [1–4]: very early age shrinkage (also called capillary or plastic shrinkage), autogenous shrinkage, carbonation shrinkage and drying shrinkage.

The very early age shrinkage takes place in fresh concrete due to transfer of moisture from the surface to the environment by evaporation and due to mass transfer from inside the concrete to the surface [5,6]. Very early age shrinkage, which is commonly measured within the first 24 h, can be avoided by an appropriate mix design and by proper curing procedures.

Autogenous shrinkage refers to the effect of volume reduction caused by cement hydration. Hence, it can be observed in sealed conditions without any moisture transfer from the concrete to the environment. For normal strength concrete with a w/c-ratio greater than 0.4 volume changes due to autogenous shrinkage are small compared to volume changes due to drying shrinkage [7–9].

The reaction between carbon dioxide and the hardened cement paste results in carbonation shrinkage. The volume reduction caused by carbonation shrinkage is very slow and is restricted to the peripheral zone. It can be neglected compared to drying shrinkage [3,10].

Drying shrinkage of concrete is the time-dependent volume decrease due to moisture migration and moisture transfer to the environment caused by a change in relative humidity. For normal strength concrete it contributes the main part of the volume change without any actions of external loads [3].

There exists a large body of literature regarding shrinkage of cementitious materials. Hansen et al. [11] investigated the influence of drying shrinkage of paste, of aggregate content and of modulus ratio of aggregates and hydrated cement on the ultimate drying shrinkage of concrete. Chaallal et al. [12] compared experimental results of drying shrinkage strains to estimated values based on ACI [13] and Euro-International Committee of Concrete (CEB) [14] recommendations. The main impetus was to compare drying shrinkage strains recorded for a large-scale concrete block with the shrinkage strains computed on the basis of the ACI and CEB codes. Bissonnette et al. [15] carried out shrinkage tests on specimens of cement pastes, mortars and concretes and evaluated the influence of different key parameters on drying shrinkage such as the size of specimens and relative humidity. In [16] Baroghel-Bouny et al. presented equilibrium and transfer moisture properties of high-performance cementitious materials and compared them with the respective properties of ordinary cement pastes and concretes. The equilibrium moisture properties of the hardened materials are described by means of water sorption isotherms, whereas the experimentally determined drying shrinkage strains are reported as function of relative humidity. Furthermore, a thermodynamic model based on the capillary curve and the intrinsic permeability of concrete was provided. After identification of the intrinsic permeability, numerically predicted moisture profiles were compared with gamma-ray attenuation measurement data. In [17] design-provisions for calculating the shrinkage and

* Corresponding author. Tel.: +43 512 507 6587; fax: +43 512 507 2908.
E-mail address: Yvonne.Theiner@uibk.ac.at (Y. Theiner).

0008-8846/$ – see front matter © 2012 Elsevier Ltd. All rights reserved.
doi:10.1016/j.cemconres.2012.06.001

creep strains of concrete from information available at the design stage, namely, the 28-day concrete strength, the concrete strength at loading, element size, and relative humidity, are presented. The combined effects of self-desiccation and "external" drying were studied experimentally in [9] by submitting concrete specimens to drying at early age. Furthermore, an experimental study on "pure" drying shrinkage, performed on a few-millimeter thick specimens of hardened cement pastes and concretes was presented. Ayano and Wittman [18] described both an experimental approach for determining the time-dependent relative humidity in the pore system of concrete and a numerical method for determining material parameters on the basis of experimental data. The hygral diffusion coefficient was expressed as function of moisture content and as function of relative humidity. Based on a phenomenological approach a model for the delayed deformations was proposed in [19]. Experimental studies highlighted the close links between delayed deformations under load and shrinkage deformations. In the authors opinion the analysis carried out leads to consideration of shrinkage as creep due to capillary stress. In [20] Videla et al. address the need to update existing concrete drying shrinkage prediction models to reflect the properties of local materials. The experimental program was carried out using eight concrete mixtures, manufactured with commonly used cements in Chile. In 2007 Baroghel-Bouny published two papers concerning water vapor sorption experiments on hardened cementitious materials [21,22]. In the first part [21] a broad range of normal and high-performance hardened cement pastes and concretes were studied under both laboratory and in-situ conditions. Water vapor desorption–adsorption experiments were carried out on very thin specimens by means of the saturated salt solution method. Furthermore, moisture profiles in structural elements exposed to various drying conditions in the laboratory and in natural environments were assessed by means of gamma-ray attenuation measurements. In order to evaluate the influence of governing parameters in the second part [22] the transport properties of various hardened cementitious materials were studied experimentally and theoretically. In [23] Bissonnette et al. described that warping and joint opening of concrete slabs in a controlled environment develop early and that the respective rate is proportional to that of drying shrinkage. The moisture changes and strains induced by water desorption of several cement based materials were studied in [24]. Experiments were conducted on ordinary mortars and cement pastes with water-to-cement ratio of 0.5 and 0.8, respectively. Finally, a numerical model, based on experimental poromechanical results, was proposed for predicting shrinkage for materials submitted to drying.

Drying shrinkage of a concrete overlay has a considerable effect on the behavior of a strengthened concrete structure. In particular, the shrinkage strains, which develop during the first days and weeks, are important for bonded concrete overlays. In [25] a computer-based design tool was presented which allows calculating the stress distribution in a bonded concrete overlay due to volume changes and restrained conditions at early age. In [26] extensive experimental measurements and numerical analyses were carried out in order to investigate the early age behavior of bonded concrete overlays. Within this time span, restrained shrinkage may result in tensile stresses, exceeding the early age tensile strength of the overlay and, hence, causing cracking of the overlay. It was found that bonded concrete overlays with high-performance concrete mixtures have a strong tendency to early-age debonding. However, as shown in [27], the tensile stresses in the overlay are reduced by stress relaxation in the overlay. Beushausen et al. [3] used composite specimens for identifying fundamental characteristics of strain development in bonded concrete overlays, considering different interface textures and overlay materials.

In an applied research project, dealing with the experimental and numerical investigation of the structural behavior of pre-damaged concrete bridge decks strengthened by concrete overlays, large-scale models, representing strips of a real bridge deck on the scale of 1:2, were tested in the laboratory [28]. Parts of the test program were simulated numerically. To this end a numerical model for concrete cracking was employed consisting of a rotating smeared crack model in combination with a crack model based on the strong discontinuity approach and formulated within the framework of finite elements with embedded discontinuities [29]. The numerical model and the numerical simulations are described in [30]. The load history, considered in the numerical simulations, consisted of (i) loading of the original test model, which induces pre-damage due to cracking, (ii) unloading, application of a concrete overlay and (iii) loading of the strengthened structure up to failure. Drying shrinkage of the concrete overlay was taken into account in the numerical simulation by the commonly employed engineering approach considering uniform shrinkage strains as initial strains. The latter were measured on concrete specimens in the laboratory, made from the concrete used for the overlay. Neglecting drying shrinkage in the numerical simulation revealed the expected influence of shrinkage of the concrete overlay on the structural behavior of the strengthened slab strip model. Expectedly, if drying shrinkage was neglected, then cracking in the overlay was initiated at a higher load level and the measured maximum crack widths were underestimated in the numerical simulation. The employed engineering approach for considering drying shrinkage of concrete overlays is characterized by the deficiency considering only a mean value of the shrinkage strains neglecting the dependence on the change of moisture distribution due to a change of relative ambient humidity.

However, for an improved representation of the drying shrinkage strains in composite structures detailed experimental data regarding the evolution of both the moisture distribution and the drying shrinkage strains in the overlay and the adjacent substrate concrete has to be determined. This task is the aim of the present contribution.

3. Experimental study

Although the shrinkage mechanisms in concrete members are well known, the effects of drying shrinkage on the performance of concrete structures strengthened by concrete overlays have not been fully clarified so far. Since drying shrinkage of a concrete overlay may have a considerable effect on the behavior of a strengthened concrete structure [25–27], it is the aim of this contribution to present a detailed experimental investigation of the effects of drying shrinkage. Whereas in [26,27] the experimental study was restricted to the overlay of composite specimens, in the present contribution the effects of drying shrinkage will be investigated beginning with hardening and drying of the original specimen, during pre-treatment of the interface by water jetting and placement of the overlay as well as during hardening and drying of the overlay.

Hence, in this contribution a comprehensive laboratory test program including (i) shrinkage tests conducted on thin concrete slices, (ii) shrinkage tests conducted on concrete prisms, (iii) shrinkage tests conducted on larger brick-shaped specimens with added concrete overlays as well as (iv) shrinkage tests conducted on reference specimens will be presented in detail. The tests focus on normal strength concrete. On the basis of the mentioned experiments the water desorption isotherm, ultimate drying shrinkage strains in terms of relative humidity, depth dependent mass water content distributions and drying shrinkage strains in terms of drying time will be determined. The measurement data will contribute to a better understanding of the role of drying shrinkage on the behavior of concrete structures strengthened by concrete overlays and will diminish the risk of shrinkage induced cracks in overlays. Hence, the experimental evaluation of the effects of drying shrinkage on the behavior of strengthened concrete structures is a first step toward the understanding of the complex structural response of concrete structures strengthened by overlays.

Table 1
Composition of concrete mix (mass proportions).

Composition	
Cement type: CEM II AM (S-L) 32,5 R	340 kg/m³
w/c-ratio	0.50
Superplasticizer type: Glenium SKY 581	0.9%
Aggregate size distribution	0/4 mm, 4/8 mm, 4/16 mm 45%, 30%, 25%

Table 2
Selected material properties at different concrete ages.

Material properties	14 days	28 days	56 days	112 days	365 days
$f_{cm,cube}$	50.0 N/mm²	55.0 N/mm²	62.0 N/mm²	74.0 N/mm²	83.0 N/mm²
f_{ctm}	4.3 N/mm²	4.8 N/mm²	5.0 N/mm²	n.a.	5.6 N/mm²
E_{cm}	35,164 N/mm²	37,483 N/mm²	39,224 N/mm²	41,188 N/mm²	41,422 N/mm²

Shrinkage tests on thin concrete slices served for determining the water desorption isotherm as well as the drying shrinkage strains in terms of ambient relative humidity. Multi-Ring-Sensors embedded in the concrete prisms were employed for determining the depth dependent moisture distribution. The test set-up for the shrinkage tests on thin concrete slices and on concrete prisms was based on [16]. However, contrary to the Multi-Ring-Sensors applied in the present investigation, in [16] the distribution of the moisture content was measured by gamma-ray attenuation. Furthermore, in the present investigation the drying shrinkage strains were also measured on the concrete prisms.

According to [3,27] different shrinkage of the substrate and the overlay significantly influence the serviceability and durability of the composite structure. Hence, in the present investigation Multi-Ring-Sensors were arranged close to the interface between brick-shaped specimens and concrete overlays providing measurement data for moisture distribution and migration in composite specimens. Comparison of the moisture distributions and shrinkage strains measured in concrete overlays and in reference specimens finally allowed evaluating the restraint effects due to the interface between the overlay and the original specimen.

The composition of the concrete mix is summarized in Table 1. Selected material parameters, as the cube compressive strength $f_{cm,cube}$, the direct uniaxial tensile strength f_{ctm} and the elastic modulus E_{cm}, determined at the age of 14 days, 28 days, 56 days, 112 days and 365 days are provided in Table 2. The mentioned material parameters represent the respective mean values determined on 5 specimens.

All specimens were moist cured for 81 days after casting. Hence, hydration can be assumed to be almost completed and autogenous shrinkage can be assumed to have attained its ultimate value at the beginning of testing.

3.1. Testing program

3.1.1. Shrinkage tests on concrete slices

For determining the water desorption isotherm and the drying shrinkage strains at different values of relative ambient humidity (RH) 10 thin concrete slices with dimensions of $110\times110\times6$ mm (Fig. 1) were submitted to drying at constant temperature of (20 ± 2)°C. Individual slices were obtained from a concrete prism with dimensions of $110\times110\times400$ mm by wet sawing. Starting at 100% RH, the RH was reduced step by step to 90%, 80%, 65% and 50%, respectively, and the corresponding equilibrium mass water contents were determined. The mass water content, representing the ratio of the mass of water in the specimen to the mass of the dry specimen (desiccated at 105 °C), was determined by weighing. Contrary to the present investigation, in [16,21] the dry reference state for calculating the mass water content was defined by the equilibrium state at 3% RH and 23 °C. However, in [21] the consequences of different definitions of the dry reference state for determining the water desorption isotherm were emphasized. Significantly higher water contents were reported in [21] when the specimens were desiccated at 105 °C. Constant mass of the specimen was assumed according to [31], i.e. when the mass changes are smaller than 0.1% of the total mass in three subsequently conducted measurements.

Each slice was equipped with 8 measuring discs highlighted by red circles in Fig. 1. They served for measuring distances along the four symmetry lines of the concrete slices as shown in Fig. 1. To this end an extensometer with a measuring accuracy of 0.003 mm and a rated measuring length of 100 mm was employed. Based on the elongations, computed from the measured distances, the respective strain was determined. As the samples were of sufficient age that autogenous shrinkage can be assumed to have attained its ultimate value (as described above), the deformations measured can be considered as drying shrinkage strains.

3.1.2. Shrinkage tests on concrete prisms

5 specimens with dimensions of $100\times100\times56$ mm (Fig. 2) were equipped with Multi-Ring Sensors (MRS, Fig. 3), temperature detectors and a number of measuring discs. In order to obtain one-dimensional moisture migration the lateral surfaces were sealed and the top and bottom face of the samples were submitted to drying at a relative humidity of (65 ± 5)% and a temperature of (20 ± 2)°C.

Multi-Ring-Sensors (MRS) [32] were applied for determining the depth dependent moisture distribution of the drying samples by measuring electrolytic resistances. Each MRS consisted of 8 measuring

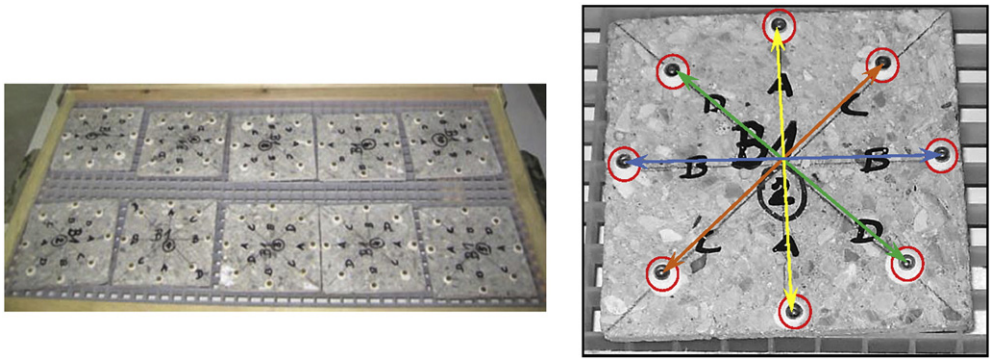

Fig. 1. Concrete slices for determining the water desorption isotherms (left) and detail of a thin concrete slice with eight measuring discs and four measurement lengths for determining the drying shrinkage strains (right).

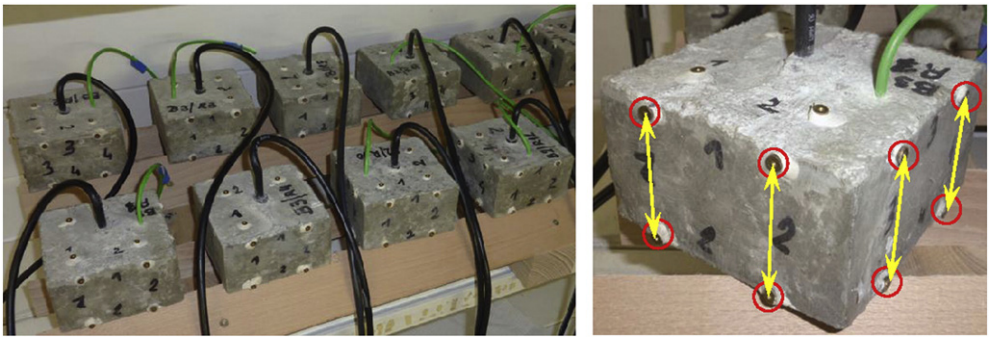

Fig. 2. Concrete prisms with sealed lateral surfaces, equipped with MRS, temperature detectors and measuring discs (left), and detail of a concrete prism with measuring discs and measurement lengths for determining the drying shrinkage strains (right).

points (MP) over a length of about 35 mm (Fig. 3). Calibration curves were used for determining the mass water content from the measured electrolytic resistances.

The drying shrinkage strains of the concrete prisms were determined using an extensometer with a rated measuring length of 50 mm. The measurement lengths are shown in Fig. 2. Since during drying the moisture distribution in the prisms is not uniform along the depth, the measured shrinkage strains represent mean values along the measuring lengths until a uniform moisture distribution was attained throughout the specimen.

3.1.3. Shrinkage tests on larger brick-shaped specimens with added overlays

In addition to the tests on thin concrete slices and concrete prisms, shrinkage tests were performed on 3 brick-shaped concrete specimens with dimensions of 800 × 300 × 300 mm, supplemented by concrete overlays with the dimensions of 800 × 300 × 90 mm on the top surface (Fig. 4). The brick-shaped specimens as well as the concrete overlays were made of the same concrete type (see Table 1). After sealing of the lateral surfaces, the top and the bottom surfaces of the specimens were submitted to drying at a relative humidity of (65 ± 5)% and a temperature of (20 ± 2)°C for more than 2 years.

The brick-shaped specimens were equipped with Multi-Ring Sensors, temperature detectors and a multitude of measuring discs. They served for measuring distances parallel to the vertical edges of the specimen with rated measuring lengths of 50 mm and 100 mm (Fig. 4). Since during drying the moisture distribution in the brick-shaped specimens is not uniform along the depth, the measured shrinkage strains represent mean values along the measuring lengths.

Fig. 5 shows the arrangement of four MRS (MRS 6 to MRS 9) used in the original concrete for one brick-shaped sample. Two of them were placed consecutively starting from the concrete surface, i.e. MRS 6 below MRS 7 and MRS 9 below MRS 8. Hence, the mass water content distribution was determined to a depth of about 80 mm below the interface.

After more than two years of drying of the brick-shaped specimens the top surfaces of two specimens were prepared by high-pressure water jetting, complying with the respective Austrian code requirements for the surface conditions of concrete structures strengthened by overlays [33]. The prepared top surfaces were covered by wet cloth for 2 days until the concrete overlay was placed. These boundary conditions were chosen in order to reproduce the strengthening procedure of existing concrete bridges in engineering practice as close as possible.

Similar to the lateral surfaces of the brick-shaped specimens also the lateral surfaces of the concrete overlays were sealed. The concrete overlays were equipped with four Multi-Ring Sensors (MRS 21 to MRS 24 in Fig. 5) and a multitude of measuring discs (Fig. 5) for measuring distances parallel to the vertical edges of the specimen with rated measuring lengths of 50 mm and of 100 mm. In order to determine the mass water content distribution through the depth of the concrete overlay two MRS were placed consecutively starting from the overlay surface, i.e. MRS 21 below MRS 22 and MRS 23 below MRS 24. The top and bottom surfaces of the composite samples

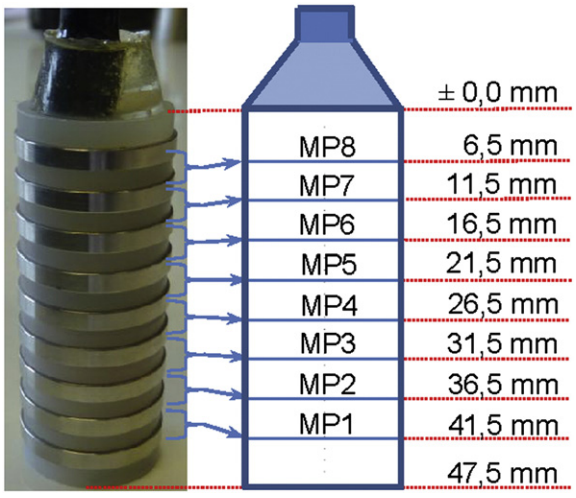

Fig. 3. Multi-Ring-Sensor (MRS) with the respective measuring points (MP) and elevations.

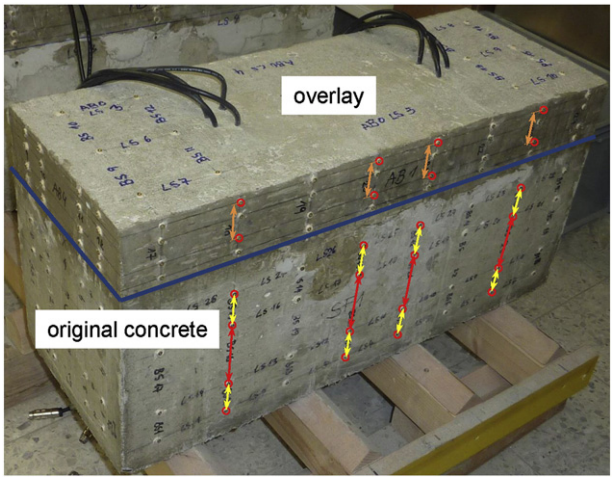

Fig. 4. Large brick-shaped concrete specimen supplemented by a concrete overlay with measuring discs and measurement lengths for determining the drying shrinkage strains.

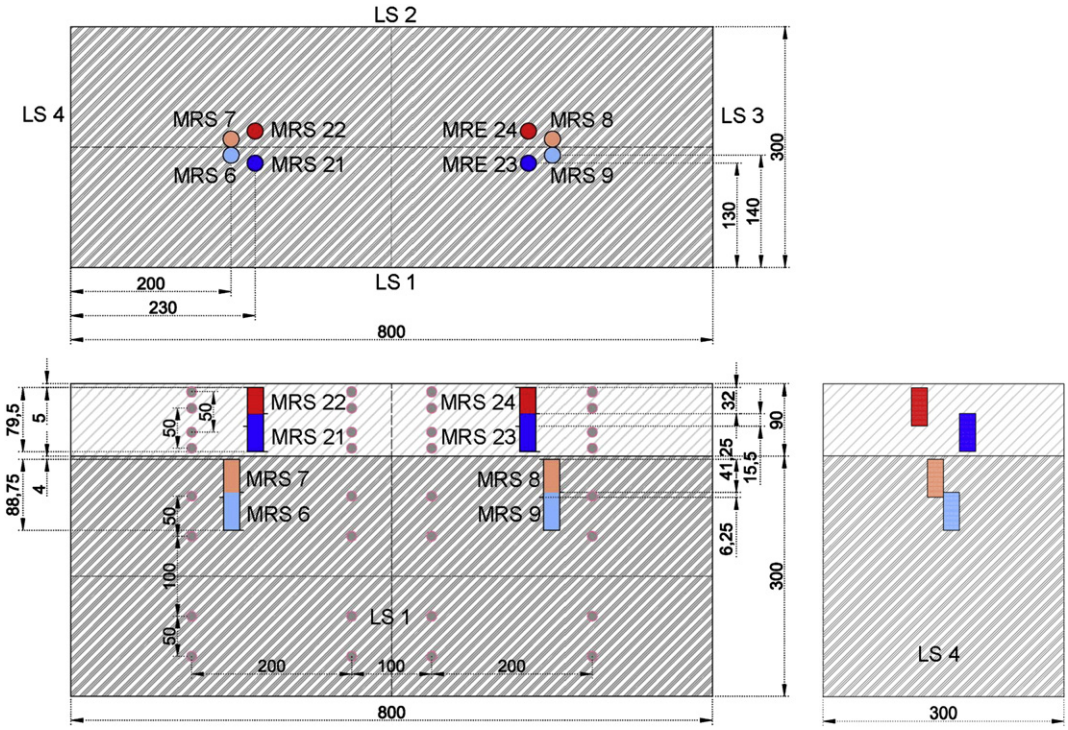

Fig. 5. Arrangement of MRS and measuring discs in the brick-shaped specimen and in the concrete overlay.

were submitted to drying at a relative humidity of (65 ± 5)% and a temperature of (20 ± 2)°C.

In [3,27] short-term and long-term tests on concrete beams with bonded concrete overlays were reported. They focused on the influence of different surface preparation methods on the micro- and macro-roughness and on the resulting restraint effects at the interface. In particular, casting the top surface of the substrate concrete against steel formwork for generating a very smooth interface, sand-blasting for roughening the interface and the application of notches at the interface for ensuring interlock between the substrate and the overlay were investigated. After surface preparation, the top surfaces were kept moist for 24 h, followed by drying for 30 to 60 min prior to the placement of the overlay. Since surface preparation by water jetting of the top surface and the evolution of the moisture distribution were not investigated in [3,27], the results are not comparable to the findings of the present study.

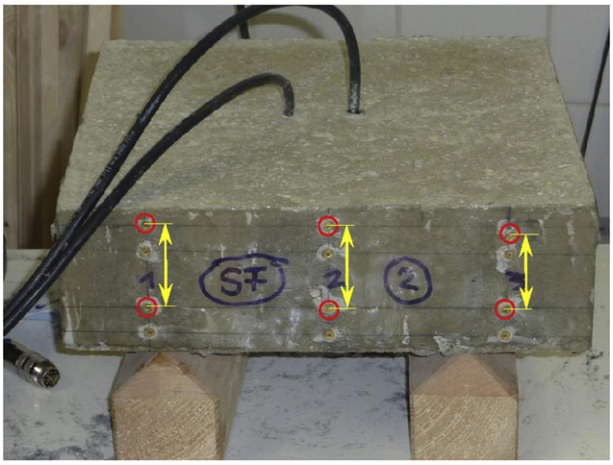

Fig. 6. Reference specimen for the concrete overlay, equipped with two MRS, measuring discs and measurement lengths.

3.1.4. Shrinkage tests on reference specimens for the overlays

In addition to the specimens mentioned so far, two so-called reference specimens for the concrete overlay with dimensions of 300 × 300 × 90 mm were cast (Fig. 6). Two MRS were embedded in each reference specimen and measuring discs were applied at the lateral surfaces.

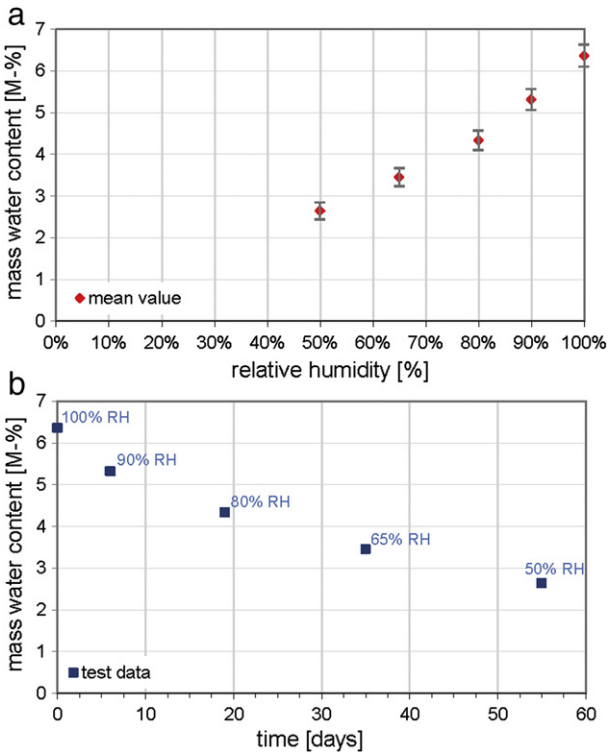

Fig. 7. Results of the tests on thin concrete slices: (a) Water desorption isotherm (mean values and standard deviation), (b) time periods for achieving sorption equilibrium at different values of relative humidity.

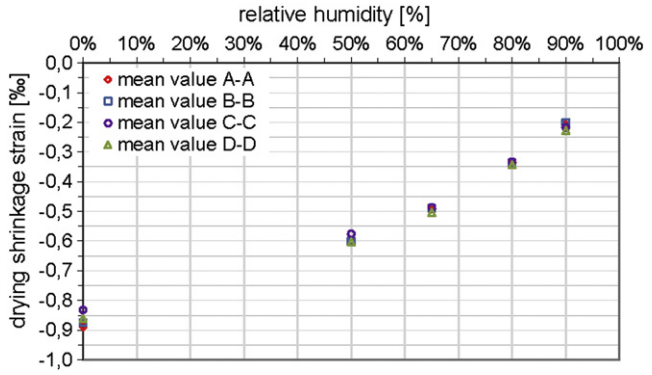

Fig. 8. Mean values of the drying shrinkage strain measured on thin concrete slices.

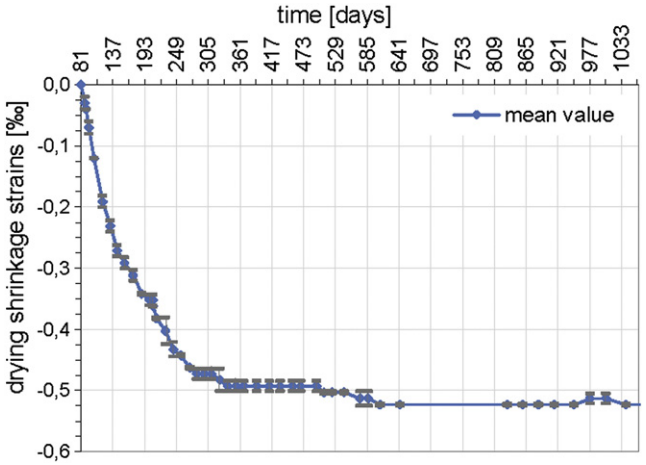

Fig. 10. Mean value and standard deviation of drying shrinkage strains measured at two sealed lateral surfaces of a concrete prism.

One of these reference specimens was sealed at the lateral surfaces and was submitted to drying at a relative humidity of $(65 \pm 5)\%$ and a temperature of $(20 \pm 2)°C$ immediately after casting. The combined autogenous and drying shrinkage strains measured for this reference specimen can thus be compared to the respective measuring data of the concrete overlay. Furthermore, comparison of the depth dependent mass water content distribution determined for the concrete overlays with the one determined for this reference specimen allows insight into the moisture migration and distribution in composite specimens.

The second reference specimen was moist cured after casting. Comparison of the measured shrinkage strains determined for both reference specimens with different curing conditions allows distinguishing between autogenous shrinkage strains on the one hand and the combined autogenous and drying shrinkage strains on the other hand.

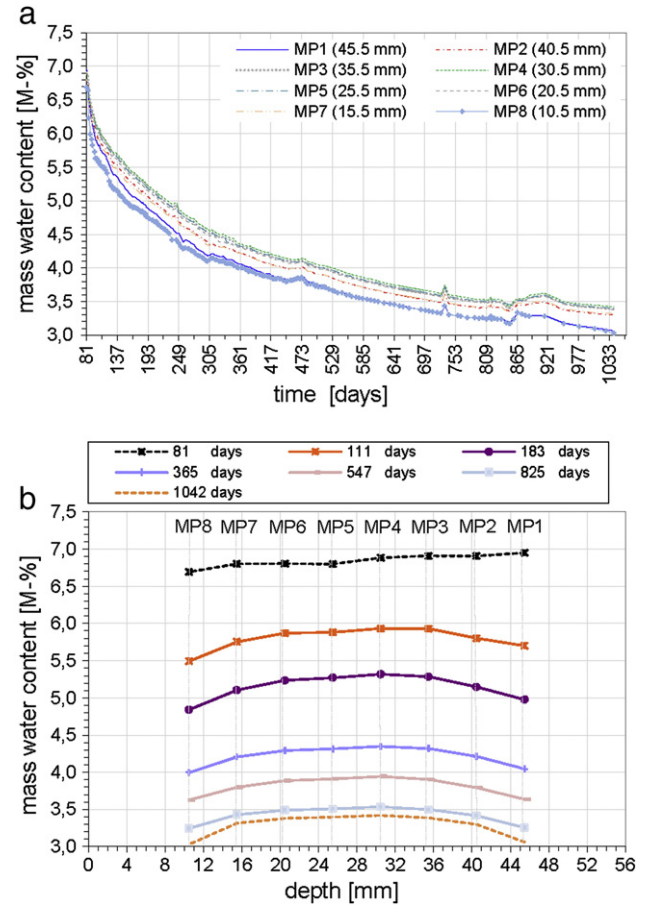

Fig. 9. Results of the tests on concrete prisms: Mass water contents at the 8 measuring points (MP) of a single MRS plotted (a) in terms of drying time and (b) along the along the center line of the specimen for selected time instants during drying.

3.2. Test results

3.2.1. Shrinkage tests on concrete slices

Fig. 7a shows the mean values and standard deviation of equilibrium mass water content for selected values of ambient relative humidity determined from the 10 thin slices shown in Fig. 1. At the end of moist curing for 81 days, i.e. at a RH of about 100%, the mean value of the measured mass water content amounted to 6.4% (standard deviation 0.25%). At a RH of 65% the mean value of the mass water content was reduced to about 3.5% (standard deviation 0.20%).

The time periods for achieving sorption equilibrium at different values of ambient relative humidity are depicted in Fig. 7b.

The mean values of the drying shrinkage strains measured on the 10 thin concrete slices in the directions A–A, B–B, C–C, and D–D (Fig. 1) are plotted in terms of ambient relative humidity in Fig. 8. There is no statistically significant difference between the respective mean values computed from the four measurement lengths A–A, B–B, C–C, and D–D. At a relative humidity of 65% the mean value of the measured drying shrinkage strain is about −0.49‰ (standard deviation 0.036‰).

The water desorption isotherm of Fig. 7a is of comparable shape as the one for a similar concrete quality reported in [16]. However, because of the different definitions of the dry state, different mix parameters and a somewhat smaller w/c-ratio, the water desorption isotherm in [16] is characterized by a lower mass water content. E.g., at 65% RH a mass water content of about 2.5% is reported in [16] compared to about 3.5% in Fig. 7a. Because of the mentioned differences in the test procedures and in the mix parameters also the drying shrinkage strains reported in [16] are smaller than those shown in Fig. 8.

3.2.2. Shrinkage tests on concrete prisms

The shrinkage tests on prismatic specimens served for determining the mass water content evolution and distribution in the samples along the length of a Multi-Ring-Sensor (MRS) in terms of drying time.

On the basis of a calibration curve, relating the measured specific electrolytic resistance to the mass water content [32], the 8 measured values of the specific electrolytic resistance for each MRS were converted to mass water contents as a function of depth. Fig. 9a shows the mass water content, i.e., the ratio of the mass of water contained in a specimen to the mass of the dry specimen, determined at the 8 measuring points (MP) of a single MRS, embedded in a concrete

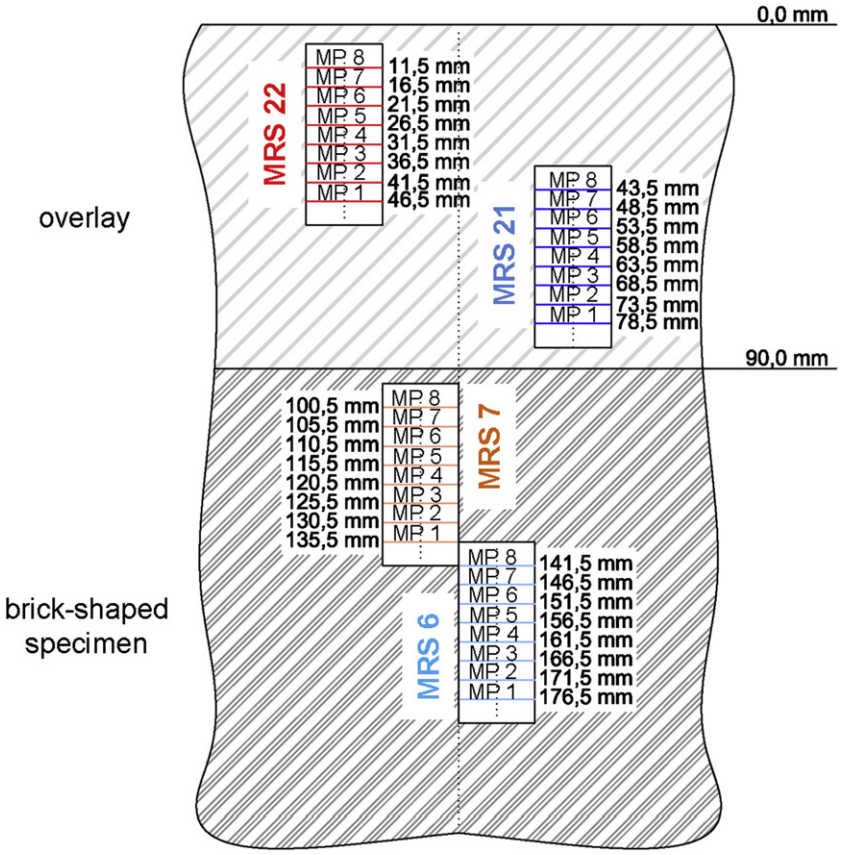

Fig. 11. Arrangement of the MRS in the composite specimen and respective elevations.

prism, as a function of drying time. In Fig. 9a the numbers in parentheses following a particular MP indicate its distance from the top surface of the concrete prism.

The mass water contents in Fig. 9a are shown, starting from the end of moist curing (81 days after casting), for a drying period of about 950 days. The mass water contents determined by the MRS (Fig. 9a) can be compared with the respective values in Fig. 7. E.g., in Fig. 7 the equilibrium mass water content of the water desorption isotherm determined at a RH of about 100% can be compared with the respective value of mass water content at the end of moist curing in Fig. 9a. The respective comparison reveals good agreement. Accordingly, in Fig. 9a the mass water content after about 950 days of drying at 65% RH is close to the equilibrium mass water content of the desorption isotherm at the respective RH, shown in Fig. 7.

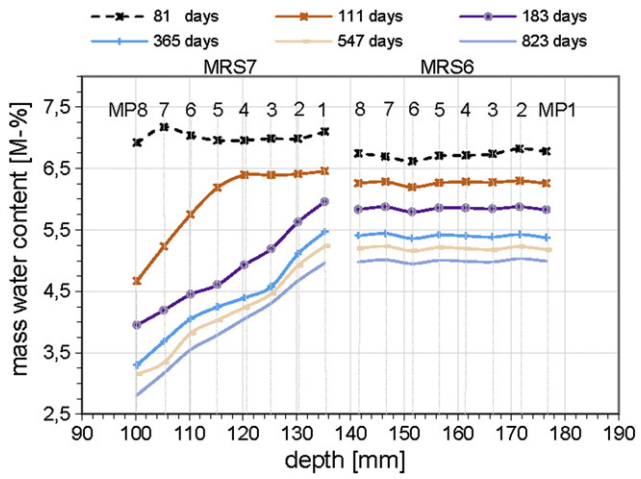

Fig. 12. Mass water content distributions in the brick-shaped specimen for selected time instants during two years of drying.

In Fig. 9b the mass water content distribution along the MRS, characterized by a measurement length of about 35 mm, is plotted for selected time instants during drying. The initial constant mass water content distribution at the end of moist curing gradually changed with progressing drying time to a distribution with decreasing values toward the surfaces due to moisture migration and moisture transfer to the environment. Furthermore, the curves in Fig. 9b mostly confirm the expected symmetry of the mass water content distribution along the center line of the specimen by comparing the measured values of mass water content of the measuring points MP1 (45.5 mm) vs. MP8 (10.5 mm), MP2 (40.5 mm) vs. MP7 (15.5 mm), MP3 (35.5 mm) vs. MP6 (20.5 mm), and MP4 (30.5 mm) vs. MP5 (25.5 mm).

The moisture content distribution and its evolution in terms of drying time can be compared with the results presented in [16] for cylindrical samples with dimension of Ø160×100 mm. They were made of normal strength concrete and were two years old at the beginning of drying. For the latter the evolution of the distribution of the moisture content, determined by gamma-ray attenuation measurements, is similar to the one in Fig. 9b, however, with a somewhat smaller decrease of the mass water content. The differences can be explained by the already mentioned different mix parameters and the different definitions of the dry reference state. The plotted distributions of the mass water content in [16] indicate the difficulty of preserving the symmetry properties of the test set-up in the test results.

The mean values of the drying shrinkage strains measured on the basis of the four measurement lengths, shown in Fig. 2, are depicted in Fig. 10. After about 950 days of drying the mean value of the

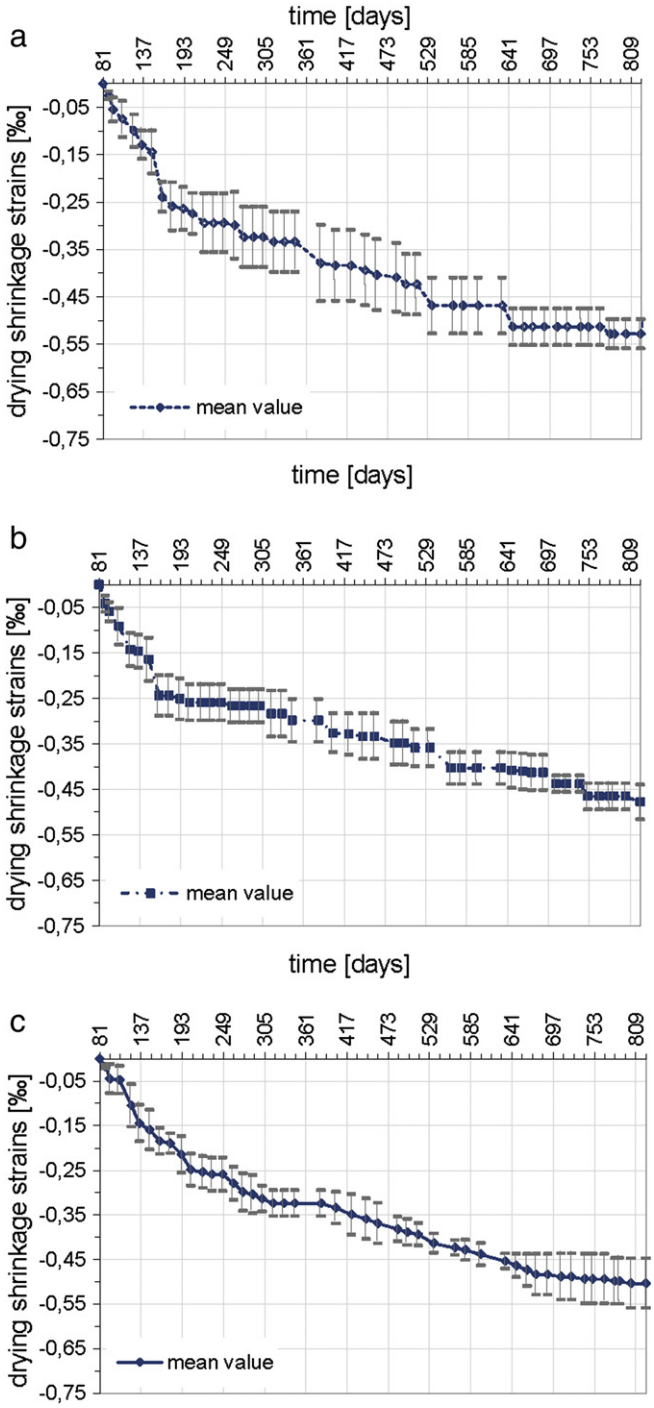

Fig. 13. Evolution of drying shrinkage strains (mean values and standard deviation) measured at (a) the upper region, (b) the middle region and (c) the lower region of the brick-shaped specimen.

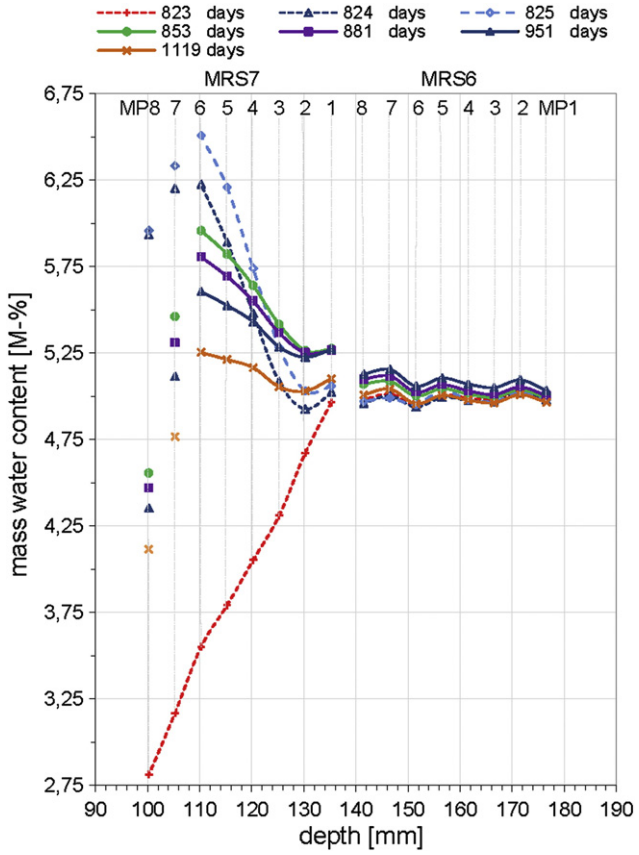

Fig. 14. Mass water content distributions in the brick-shaped specimen at the last day of drying (t = 823 days), after surface preparation during subsequent wetting of the top surface (t = 824 days), before placement of the overlay (t = 825 days) up to 294 days after placement of the overlay (t = 1119 days).

measured shrinkage strains amounted to about −0.52‰ (standard deviation 0.003‰).

The evolution of the shrinkage strains, shown in Fig. 10, qualitatively agrees quite well with the evolution of shrinkage strains reported in [15] for specimens with dimension of 50 × 50 × 400 mm made of normal strength concrete with a w/c-ratio of 0.5. The latter were moist cured for 28 days, followed by drying at 48% RH. The ultimate shrinkage strain of −0.65‰ was larger than the one in Fig. 10. The differences are the result of different mix properties, of a lower value of ambient RH and of different concrete ages at the beginning of drying. According to the shrinkage curves plotted in Fig. 10 and in [15] the evolution of the shrinkage strains, requiring about 200 days of drying for obtaining 90% of the ultimate shrinkage strain, is considerably slower than for smaller concrete specimens.

3.2.3. Shrinkage tests on larger brick-shaped specimens

The depth dependent mass water content distribution in the larger brick-shaped specimens was determined by means of MRS in a similar manner as in the shrinkage tests on concrete prisms. The lower part of Fig. 11 shows the arrangement of MRS 7 and MRS 6 in the brick-shaped specimen of Fig. 5. In Fig. 12 the mass water content distribution is plotted for selected times along the two consecutively placed MRS 7 and MRS 6 in one of the brick-shaped specimens. The mass water contents in the brick-shaped specimen, shown in Fig. 12, were measured during drying until the top surface of the specimen was prepared by high-pressure water jetting, as described in Section 3.1.3. Ideally, at the end of moist curing (t = 81 days) the measured mass water content should be uniform throughout the specimen. The measured deviations from the expected uniform distribution can be attributed to different degrees of compaction of the concrete through the specimen depth. The measured values of MRS 6 show a uniform decrease of the mass water content in the inner region of the brick-shaped concrete specimen, i.e. at distances from the surface larger than about 50 mm (Fig. 11), from initially 6.75% to 5.4% after 1 year of drying. During the second year of drying the latter value decreased to 5.0%.

By contrast, in the near-surface region the mass water content during drying, described by the measuring values of MRS 7 in Fig. 12, decreases toward the top surface, resulting in a decrease of

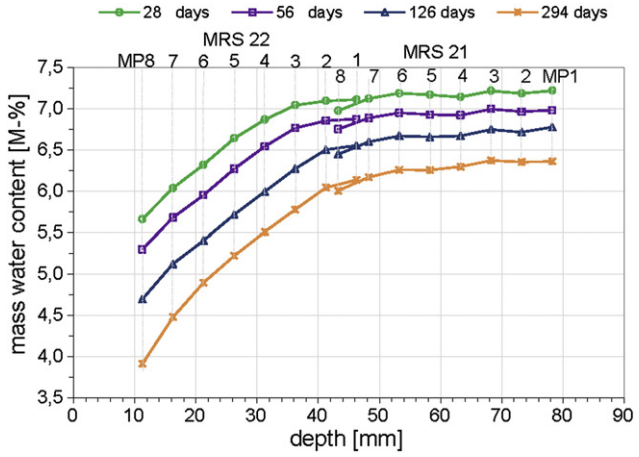

Fig. 15. Mass water content distributions in the added concrete overlay for selected time instants.

the initial water content of 7.0% at the end of moist curing to 2.8% near the surface after more than two years of drying.

The mean values of the drying shrinkage strains, measured on the basis of the measurement lengths, shown in Fig. 4, are depicted in Fig. 13. The shrinkage strains measured at the upper and lower region of the brick-shaped specimen attained the expected final value of about −0.5‰ (standard deviations of 0.03‰ and 0.05‰, respectively) after about 600 days of drying at 65% RH. Expectedly, in the middle region of the specimen the evolution of the drying shrinkage strain (standard deviation 0.03‰) was somewhat delayed with respect to the upper and lower region.

3.2.4. Shrinkage tests on larger brick-shaped specimens with added overlays

In Fig. 14 the mass water content distributions in a brick-shaped specimen are plotted for selected time instants along the consecutively placed MRS 7 and MRS 6, starting from the last day of drying immediately before preparation of the top surface by high-pressure water jetting (t = 823 days), 24 h after water jetting (t = 824 days), immediately before placement of the concrete overlay (t = 825 days) until 294 days after placement of the concrete overlay (t = 1119 days). From water jetting until placement of the overlay at t = 825 days the top surface of the brick-shaped specimen was covered by wet cloth, protected by a plastic foil.

High-pressure water jetting removes concrete from the top surface down to a depth of a few millimeters below the original surface and cracks are produced in the superficial zone extending to a depth of several millimeters [34,35]. Hence, application of the calibration curve for determining the mass water content from the electrolytic resistances measured by the MRS is questionable for the superficial zone of the brick-shaped specimen. For this reason the mass water contents measured at measurement points MP8 and MP7 of MRS 7 are indicated only by dots and are not connected to the plotted distributions below the superficial zone.

Whereas the mass water content of about 5% measured at measurement point MP1 of MRS 6 in the inner region of the brick-shaped specimen remained almost constant during high-pressure water jetting and subsequent wetting of the top surface of the brick-shaped specimen, the measurement points of MRS 7, placed closer to the top surface of the brick-shaped specimen, showed a distinctive change in mass water content. Due to water jetting and subsequent wetting of the top surface of the brick-shaped specimen the mass water content at MP6 of MRS 7 increased from 3.6% at the end of drying (t = 823 days) up to about 6.5%.

After placement of the overlay in the region close to the interface the mass water content in the old concrete is decreasing by water migration toward the interior of the brick-shaped specimen. In the interior of the brick-shaped specimen a delayed increase of the mass water content is observed (up to t = 951 days), followed by a decrease toward the original mass water content of 5%, measured before surface preparation and placement of the concrete overlay.

For the concrete overlay the mass water content distribution is shown for selected time instants in Fig. 15. The mass water contents of the concrete overlay close to the interface, measured by the measurement points MP1 to MP3 of MRS 21, show a uniform decrease from about 7.2% after 28 days of drying to about 6.3% after 294 days of drying, whereas the measuring points MP4 to MP8 of MRS 21 indicate a slight decrease of the mass water content toward the surface of the overlay. By contrast, the mass water content distribution in the near-surface region, represented by the measuring values of MRS 22, is characterized by a steep gradient, resulting at MP8 of MRS 22 in a decrease of the mass water content from 5.7% after 28 days of drying to 3.9% after 294 days of drying.

The evolution of the drying shrinkage strains for the brick-shaped specimen is shown in Fig. 16 in terms of the mean values measured at a lateral surface in the upper, middle and lower region, respectively, as a function of drying time. The mean values were determined from four measurements along the length of the specimen shown in Fig. 4. The red arrow in Fig. 16 indicates the time instant, when the top surface of the brick-shaped specimen was prepared by high-pressure water jetting. Expectedly, Fig. 16 clearly shows that in the lower region of the brick shaped specimen the evolution of the shrinkage strains was not affected by surface preparation and placement of the overlay. In the middle region of the specimen the

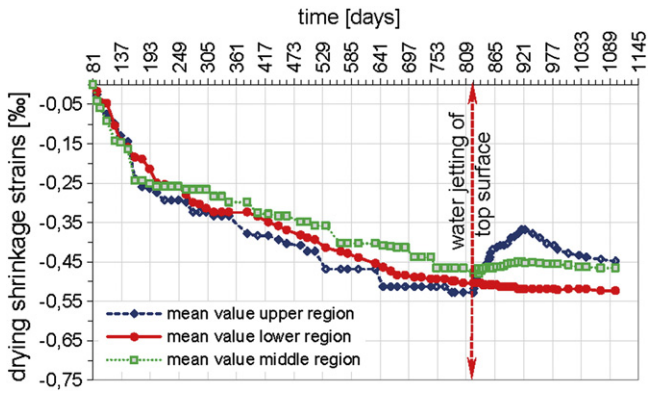

Fig. 16. Mean values of drying shrinkage strains measured at the upper, middle and lower region of a lateral surface of the brick-shaped specimen.

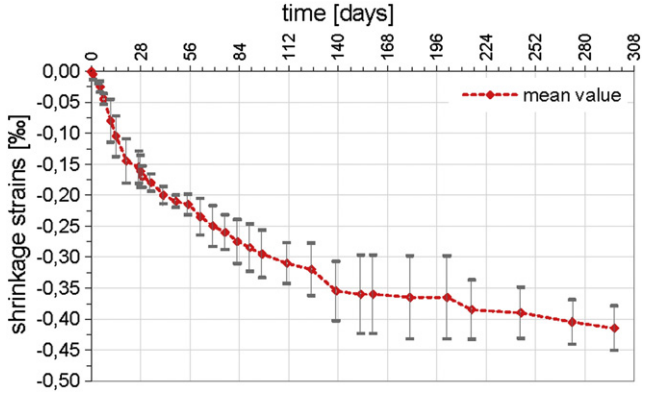

Fig. 17. Mean value and standard deviation of shrinkage strains measured at a lateral surface of the concrete overlay.

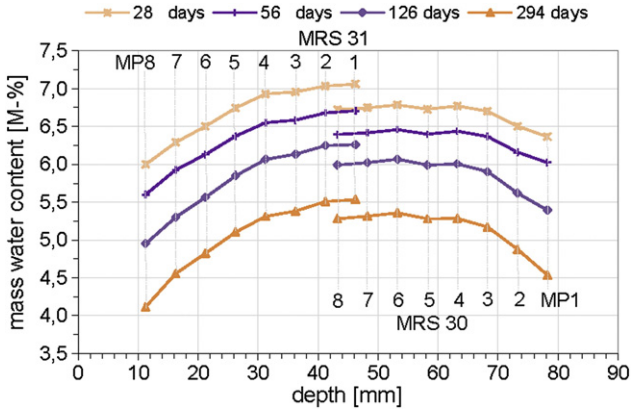

Fig. 18. Mass water content distributions in the reference specimen submitted to drying immediately after casting.

evolution of the drying shrinkage strains did not change significantly after surface preparation and casting of the concrete overlay. By contrast, the evolution of the shrinkage strains in the upper region was strongly influenced. The increased mass water content near the surface of the brick-shaped specimen, indicated by the measurement values of MRS 7 in Fig. 14, resulted in a delayed increase in mass water content in the region below MRS 7 (according to the measurement values of MRS 6 in Fig. 14). Thus, the shrinkage strains in the upper region of the brick-shaped specimen decreased as shown in Fig. 16.

The mean values of the shrinkage strains measured at a lateral surface of the concrete overlay are shown in Fig. 17. The diagram represents the mean values determined from the four measurements along the length of the overlay, shown in Fig. 4. Because the concrete overlay was submitted to drying at a relative humidity of (65 ± 5)% and a temperature of (20 ± 2)°C immediately after removing the formwork, the strains shown in Fig. 17 represent the combination of autogenous and drying shrinkage strains. Furthermore, they are affected by the restraint effects exerted from the old concrete to the overlay.

3.2.5. Shrinkage tests on reference specimens

As described in Section 3.1.4, in addition to the added overlays the two so-called reference specimens were produced. For the reference specimen submitted to drying immediately after casting, Fig. 18 depicts the mass water content distributions at selected time instants for the two consecutively placed MRS 31 and MRS 30. Comparison of the measurement values of MRS 31 and MRS 30 reveals deviations from the expected symmetric distribution of the mass water content through the depth. They can be explained by difficulties in maintaining the exact positions of the MRS during placement and compaction of the concrete. After 28 days of drying, moisture migration and moisture transfer to the environment resulted in decreasing values of the mass water content toward the surfaces. From 28 days to 294 days of drying, in the near-surface regions the water content decreased from 6.0% to 4.1% at MP8 of MRS 31 and from 6.3% to 4.5% at MP1 of MRS 30, respectively.

The evolution of the combined autogenous and drying shrinkage strains, measured at a sealed lateral surface of the reference specimen, submitted to drying immediately after casting, is shown in Fig. 19. The diagram represents the mean values determined from the three measurements along the length of the reference specimen shown in Fig. 6.

For the second reference specimen the mass water content distribution is shown for selected time instants during moist curing in Fig. 20. The recorded values of MRS 32 and MRS 33 for the mass water content show a nearly uniform decrease from about 7.5% to about 6.3%.

The mean values of shrinkage strains measured at a lateral surface of the reference specimen after 81 days of moist curing amounted to about −0.08‰. The latter are autogenous shrinkage strains. As expected, they are small compared to the shrinkage strains measured on the reference specimen submitted to drying immediately after casting.

In [9] the effects of combined self-desiccation and external drying were investigated by submitting concrete specimens made of normal strength concrete with dimensions of $70\times70\times280$ mm to drying at (65 ± 5)% RH one day after casting. Simultaneously, autogenous shrinkage strains were measured on sealed specimens. The reported autogenous shrinkage strain of about −0.12‰ is larger than the one of the present investigation. However, the total shrinkage strain reported in [9] is of similar magnitude as the total shrinkage strain measured on the reference specimen in the present investigation. The moisture distribution determined by means of capacitive probes on drying samples of normal strength concrete with dimensions of $150\times150\times300$ mm in [9] can be compared with the mass water content distributions in the reference specimen submitted to drying immediately after casting shown in Fig. 18. Qualitatively, the reported decrease of mass water content in [9] agrees with the one plotted in Fig. 18.

3.3. Interpretation of the test results for the composite specimen

Fig. 21, which is composed of Figs. 15 and 14, from left to right depicts the distributions of the mass water content from the surface of the overlay to the interior region of the original brick-shaped specimen from the last day of drying ($t=823$ days) of the brick

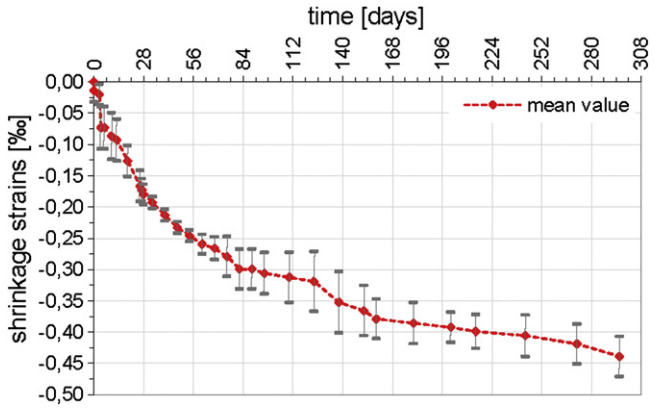

Fig. 19. Mean value and standard deviation of combined autogenous and drying shrinkage strains measured at a lateral surface of a reference specimen, submitted to drying immediately after casting.

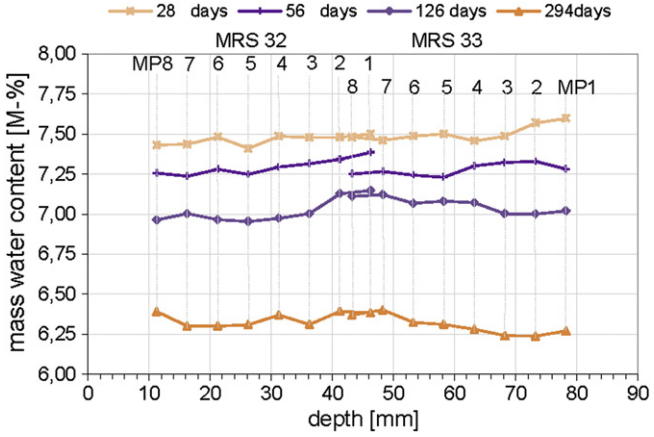

Fig. 20. Mass water content distributions in the reference specimen for selected time instants during moist curing.

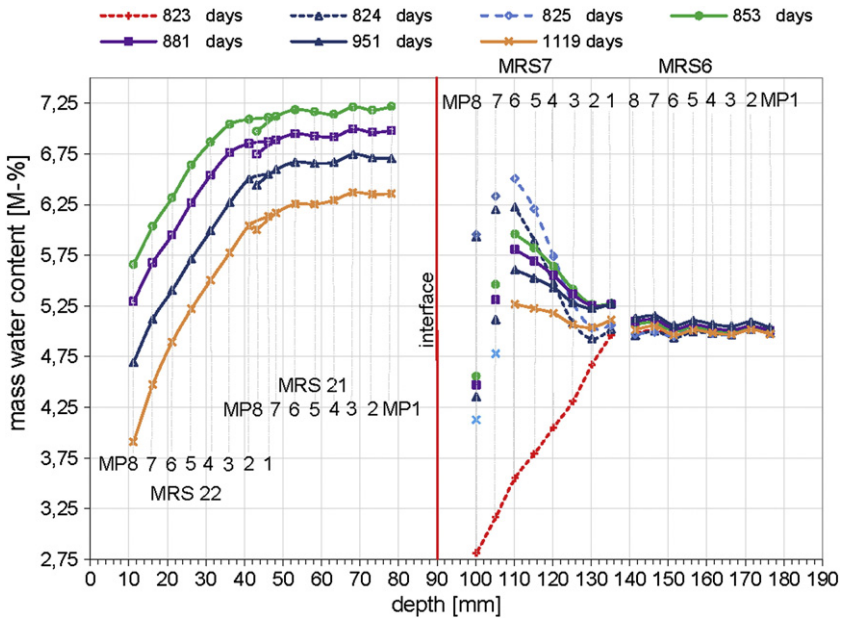

Fig. 21. Mass water content distributions from the surface of the overlay to the interior region of the brick shaped specimen at selected time instants.

shaped specimen until 294 days after placement of the overlay (t = 1119 days). Since the overlay was placed at t = 825 days, the four curves for the mass water content in the overlay refer to overlay ages of 853 days–825 days = 28 days, 881 days–825 days = 56 days, 951 days–825 days = 126 days and 1119 days–825 days = 294 days, respectively. Comparison of the peak value of the mass water content of 6.5%, measured in the old concrete at MP6 of MRS 7 after water jetting and wetting of the top surface, with Fig. 12 reveals that the peak value of 6.5% is close to the mass water content of 7% in the brick-shaped specimen at the end of moist curing. After the placement of the concrete overlay, water was migrating in the old concrete from the wetted region at the interface toward the interior of the brick-shaped specimen. This is indicated by the gradient of the mass water content along MRS 7 and the slight gradient along MRS 6, which decreases only at later stages (t > 951 days, see also Fig. 14). The time-dependent changes in mass water content of the old concrete resulted in a delayed decrease of the shrinkage strains in the upper region of the brick-shaped specimen. This follows from Fig. 16 for t > 825 days, where the measured shrinkage strains in the upper region of the brick shaped specimen refer to the measurement length ranging from 50 mm to 100 mm below the interface (as shown in Fig. 5), which corresponds to the range of MRS 6 in Fig. 21.

In the overlay the time-dependent decrease of the mass water content, shown in Fig. 21, indicates water migration toward the surface of the overlay. Since the decrease of the mass water content in the overlay is caused by both hydration and drying, the shrinkage strains, shown in Fig. 17, represent combined autogenous and drying shrinkage strains. In addition, they are influenced by restraint effects exerted from the interface on the deformations of the overlay. Comparison of Figs. 17 and 19, the latter depicting the combined autogenous and drying shrinkage strains measured on the reference specimen submitted to drying immediately after casting, reveals that the shrinkage strains in the concrete overlay are smaller than the ones in the reference specimen. However, the difference is small. This fact indicates relatively small restraint effects exerted from the old concrete on the deformations of the overlay. This desirable effect was achieved by thorough wetting of the superficial zone of the old concrete, which results in a decrease of the shrinkage strains, related to the maximum value of the shrinkage strains due to previous drying. During subsequent drying of the overlay, according to Fig. 21 decreasing values of the mass water content are observed in both the overlay and the superficial zone of the old concrete. They result in the simultaneous evolution of shrinkage strains in the overlay and re-increase of shrinkage strains in the old concrete close to the interface. The simultaneous evolution of shrinkage strains in the overlay and the adjacent old concrete reduces restraint effects at the interface.

Comparison of the evolution of the mass water content for the reference specimen, submitted to drying immediately after casting, in Fig. 18 with the respective values for the near-surface region of the concrete overlay in Fig. 15 shows similar behavior close to the surface. Expectedly, in the interior region of the overlay the mass water content decrease is lower than in the reference specimen, since in the latter also the bottom surface was exposed to drying.

4. Summary and outlook

It was the aim of this contribution to investigate the effects of drying shrinkage on the behavior of concrete structures strengthened by overlays. Normal strength concrete was used for both the original concrete and the concrete overlay. Thin concrete slices served for determining the shrinkage strains in terms of ambient relative humidity and the water desorption isotherm, characterizing the equilibrium moisture properties of the selected concrete. Depth dependent moisture distribution profiles were determined by measuring electrolytic resistances by means of Multi-Ring-Sensors, placed in concrete prisms with sealed lateral surfaces for enforcing one-dimensional moisture transport. Furthermore, the drying shrinkage strains were measured on the lateral surfaces of the concrete prisms. The measurements by the Multi-Ring-Sensors were verified by comparing the equilibrium mass water contents, determined by means of step-by-step desorption, with the respective mass water contents determined by the Multi-Ring-Sensors.

In addition to the lab tests for determining the hygral and mechanical properties of the employed concrete, tests on larger brick-shaped specimens supplemented by concrete overlays were performed. Multi-Ring-Sensors were placed in the near-surface region of the brick-shaped concrete specimen for monitoring the depth dependent moisture distribution during drying for more than two years, during surface preparation by high-pressure water jetting and subsequent wetting of the interface by wet cloth and after placement

of the concrete overlay. Moreover, the shrinkage strains were recorded in the brick-shaped specimens and in the added concrete overlay. In the overlay the mass water content decreased due to hydration and drying. Both effects resulted in shrinkage strains. In the upper zone of the old concrete, firstly wetting induced a delayed decrease of the shrinkage strains, referred to those from previous drying, followed by a re-increase of the shrinkage strains due to water migration to interior regions of the old concrete. The simultaneous increase of shrinkage strains in the overlay and in the old concrete close to the interface reduced restraint effects at the interface. This conclusion was confirmed by similar evolutions of the combined autogenous and drying shrinkage strains in the overlay and in the reference specimen submitted to drying immediately after casting.

Firstly, the findings of this investigation contribute to a better understanding of the impact of surface preparation and of drying shrinkage on the behavior of concrete structures strengthened by concrete overlays.

Secondly, extensive experimental data is provided for calibrating and validating numerical models for drying shrinkage. The test data from the thin concrete slices and the concrete prisms can be used for the former task, whereas for the latter task the test results from the composite specimens can be employed. In a further investigation the results of the presented laboratory tests will be used for calibrating and validating two models for drying shrinkage. The first one is a simplified model, available in commercial FE-programs, which relates the shrinkage strain to the change in relative humidity by a shrinkage parameter [36]. The latter is based on a three-phase model for concrete taking into account the physical origin of drying shrinkage, which is related to the increase of the capillary pressure in the concrete with decreasing relative pore humidity during the drying process [37].

Thirdly, the test results reveal possible improvements of the test setup for the composite specimens. In the tests of the present investigation Multi-Ring-Sensors were not placed across the interface because of the large risk of damage of the sensors during high-pressure water jetting and because of the questionable application of the calibration curve for converting measured electrolytic resistances to mass water contents in the superficial zone, in which cracks are produced by water jetting. However, this region is of considerable interest. Hence, future attempts should be aiming at measurement data in the regions very close to the interface between the old and new concrete.

Acknowledgment

Financial support for this research project by the Tyrolean Science Fund is gratefully acknowledged.

References

[1] P. Acker, Shrinkage stresses in fracture mechanics of concrete structures — from theory to applications, in: L. Elfgren (Ed.), Report of the Technical Committee 90-FMA Fracture Mechanics to Concrete-Applications, RILEM, Chapman and Hall, London, 1989, pp. 155–161.
[2] R. Le Roy, F. de Larrard, Creep and shrinkage of high-performance concrete: the LCPC experience, in: Z. Bažant, I. Carol (Eds.), Proceedings of the Fifth International RILEM Symposium in Barcelona, E&FN Spon, London, 1993, pp. 499–504.
[3] H. Beushausen, Long-term performance of bonded concrete overlays subjected to differential shrinkage. Ph.D. thesis, University of Cape Town, South Africa, 2005.
[4] K.H. Khayat, W.J. Long, Shrinkage of precast, prestressed self-consolidating concrete, ACI Mater. J. 107 (2010) 231–237.
[5] P. Turcry, A. Loukili, Evaluation of plastic shrinkage cracking of self-consolidating concrete, ACI Mater. J. 103 (2006) 272–279.
[6] N.K. Emberson, G.C. Mays, Significance of property mismatch in the patch repair of structural concrete. Part 1: properties of repair systems, Mag. Concr. Res. 42 (1990) 147–160.
[7] E. Tazawa, S. Miyazawa, Autogenous shrinkage of concrete and its importance in concrete technology, in: Z. Bažant, I. Carol (Eds.), Proceedings of the Fifth International RILEM Symposium in Barcelona, E&FN Spon, London, 1993, pp. 159–168.
[8] M.-H. Zhang, L. Li, P. Paramasivam, Shrinkage of high-strength lightweight aggregate concrete exposed to dry environment, ACI Mater. J. 102 (2005) 86–92.
[9] V. Baroghel-Bouny, J. Godin, Experimental study on drying shrinkage of ordinary and high-performance cementitious materials, Concr. Sci. Eng. 3 (2001) 13–22.
[10] M.G. Alexander, Deformation and volume change of hardened concrete, Fulton's Concrete Technology, 8th edn, 2001, Midrand, South Africa.
[11] W. Hansen, J.A. Almudaiheem, Ultimate drying shrinkage of concrete — influence of major parameters, ACI Mater. J. 84 (1987) 217–223.
[12] O. Chaallal, B. Benmokrane, G. Ballivy, Drying shrinkage strains: experimental versus codes, ACI Mater. J. 89 (1992) 263–266.
[13] ACI Committee 209, Prediction of creep, shrinkage, and temperature effects in concrete structures, Designing for Creep and Shrinkage in Concrete Structures, SP-76, American Concrete Institute, Detroit, 1982, pp. 193–300.
[14] Model Code for Concrete Structures, Bulletin d'Information 124/125E, Comité Euro-Internationale du Béton/Fédération Internationale de la Précontrainte, Paris, 1978.
[15] B. Bissonnette, P. Pierre, M. Pigeon, Influence of key parameters on drying shrinkage of cementitious materials, Cem. Concr. Res. 29 (1999) 1655–1662.
[16] V. Baroghel-Bouny, M. Mainguy, T. Lassabatere, O. Coussy, Characterization and identification of equilibrium and transfer moisture properties for ordinary and high-performance cementitious materials, Cem. Concr. Res. 29 (1999) 1225–1238.
[17] N.J. Gardner, M.J. Lockmann, Design provisions for drying shrinkage and creep of normal-strength concrete, ACI Mater. J. 98 (2001) 159–167.
[18] T. Ayano, F.H. Wittmann, Drying, moisture distribution, and shrinkage of cement-based materials, Mater. Struct. - Sci. Rep. 35 (2002) 134–140.
[19] G. Pons, P. Munoz, G. Escadeillas, Determination of concrete total deformations under load as function of shrinkage value, ACI Mater. J. 100 (2003) 14–20.
[20] C. Videla, J.P. Covarrubias, C. Masana, Updating concrete drying-shrinkage prediction models for local materials, ACI Mater. J. 101 (2004) 187–198.
[21] V. Baroghel-Bouny, Water vapour sorption experiments on hardened cementitious materials: Part I: essential tool for analysis of hygral behaviour and its relation to pore structure, Cem. Concr. Res. 37 (2007) 414–437.
[22] V. Baroghel-Bouny, Water vapour sorption experiments on hardened cementitious materials: Part II: essential tool for assessment of transport properties and for durability predictions, Cem. Concr. Res. 37 (2007) 438–454.
[23] B. Bissonnette, E.K. Attiogbe, M.A. Miltenberger, C. Fortin, Drying shrinkage, curling, and joint opening of slabs-on-ground, ACI Mater. J. 104 (2007) 259–267.
[24] T. Rougelot, F. Skoczylas, N. Burlion, Water desorption and shrinkage in mortars and cement pastes: experimental study and poromechanical model, Cem. Concr. Res. 39 (2009) 36–44.
[25] D.A. Lange, H.-C. Shin, A computer-based design tool for analysis of bonded concrete overlays, Concr. Sci. Eng. 3 (2001) 189–194.
[26] H.-C. Shin, D.A. Lange, Effects of shrinkage and temperature in bonded concrete overlays, ACI Mater. J. 101 (2004) 358–364.
[27] H. Beushausen, M.G. Alexander, Failure mechanisms and tensile relaxation of bonded concrete overlays subjected to differential shrinkage, Cem. Concr. Res. 36 (2006) 1908–1914.
[28] J. Feix, A. Andreatta, C. Niederegger, G. Fritsche, G. Hofstetter, G. Niederwanger, Y. Theiner, T. Cordes, Composite constructions used for load-bearing structures and roadways of bridges, Research Report, Published in Scientific Series of Research (Straßenforschungsheft Nr. 589), Federal Ministry of Traffic, Innovation and Technology, Vienna, Austria, 2010, in German.
[29] Y. Theiner, G. Hofstetter, Numerical prediction of crack propagation and crack widths in concrete structures, Eng. Struct. 31 (2009) 1832–1840.
[30] Y. Theiner, G. Hofstetter, A crack model with delayed embedded discontinuities for the numerical prediction of crack widths in concrete structures, Proceedings of the 9th International Conference on Computational Structures Technology (CST2008), Athens, Greece, 2008, CD-ROM, 18 pp.
[31] EN ISO 12571, Hygrothermal performance of building materials and products — determination hygroscopic sorption properties, ICS 91.100.01, 2000, in German.
[32] W. Brameshuber, M. Raupach, P. Schröder, C. Dauberschmidt, Non-destructive determination of the water-content in the concrete cover using the multiring-electrode, Proceedings of the International Symposium Non-Destructive Testing in Civil Engineering (NDT-CE), Berlin, Deutsche Gesellschaft für Zerstörungsfreie Prüfung, DGZfP, Berlin, 2003, 14 pp.
[33] Guideline RVS 15.02.34, Bridges: design and detailing of concrete overlays, Draft 20.01.2010, Austrian Research-Promotion Agency Road–Rail Traffic, 2010, in German.
[34] B. Bissonnette, L. Courard, A.M. Vaysburd, A.N. Belair, Concrete removal techniques, Concr. Int. 28 (2006) 49–55.
[35] L. Courard, J.-F. Lenaers, Evaluation of saturation and microcracking of the superficial zone of concrete, Concrete Repair, Rehabilitation and Retrofitting II, Taylor & Francis, London, 2009, pp. 977–982.
[36] A. Van Beek, E. Schlangen, Simulating the effect of shrinkage on concrete structures, in: V. Baroghel-Bouny, P.C. Aitcin (Eds.), RILEM Proceedings PRO 17 Shrinkage of Concrete, Shrinkage 2000, 2000, pp. 477–492.
[37] D. Gawin, F. Pesavento, B.A. Schrefler, Hygro-thermo-chemo-mechanical modelling of concrete at early ages and beyond; part I: hydration and hygro-thermal phenomena, part II: shrinkage and creep of concrete, Int. J. Numer. Methods Eng. 67 (2006) 299–363.